355 nm Multiphoton Dissociation and Ionization of 2, 5-Dihydroxyacetophenone†

Yuri A. Dyakov, Shang-Ting Tsai, Arnab Bagchi,‡ Chien-Ming Tseng,§ Yuan T. Lee,‖ and Chi-Kung Ni⊥,*

Institute of Atomic and Molecular Sciences, Academia Sinica, P.O. Box 23-166, Taipei, 10617 Taiwan

Received: May 31, 2009; Revised Manuscript Received: September 1, 2009

Multiphoton dissociation and ionization of 2,5-dihydroxyacetophenone (DHAP), an important matrix compound in UV matrix-assisted laser desorption/ionization (MALDI), is studied in a molecular beam at 355 nm using multimass ion imaging mass spectrometer and time-of-flight mass spectrometry. For laser fluence larger than 130 mJ/cm^2, nearly all of the irradiated molecules absorb at least one photon. The absorption cross section was found to be $\sigma = 1.3(\pm 0.2) \times 10^{-17}$cm^2. Molecules excited by two photons quickly dissociate into fragments. The major channels are (1) $C_6H_3(OH)_2COCH_3 \rightarrow C_6H_3(OH)_2CO + CH_3$ and (2) $C_6H_3(OH)_2COCH_3 \rightarrow C_6H_3(OH)_2 + COCH_3$. Molecules absorbing three or more photons become parent ions or crack into smaller ionic fragments. The concentration ratio of ions (parent ions and ionic fragments) to neutral fragments is about 10^{-6}:1. Changing the molecular beam carrier gas from He at 250 Torr to Ar at 300 Torr results in molecular beam clustering (dimers and trimers). Multiphoton ionization of clusters by a 355 nm laser beam produces only dimer cations, $(C_6H_3(OH)_2COCH_3)_2^+$. Protonated clusters or negatively charged ions, observed from a solid sample of DHAP using 355 nm multiphoton ionization, were not found in the molecular beam. The experimental results indicate that the photoionization occurs in the gas phase after DHAP vaporizes from the solid phase may not play an important role in the MALDI process.

I. Introduction

The compound, 2,5 dihydroxyacetophenone (DHAP) is frequently used as a matrix compound in UV matrix-assisted laser desorption/ionization (MALDI).[1] MALDI is regularly used for peptide and protein analysis. Although the details of mechanism are not well understood, several mechanisms have been proposed.[2−4] Photochemical ionization is one of the proposed MALDI mechanisms.[2] In this mechanism, photoionization of matrix molecules is considered the primary process for subsequent ionization of the analyte in the gas phase. However, several processes can compete with photoionization after irradiation with UV photons. They include energy transfer and proton transfer between DHAP and dissociation. Although DHAP is commonly used as the matrix compound for ultraviolet MALDI, the photochemistry of DHAP remains unclear.

We previously investigated DHAP photodissociation in a molecular beam at 193 nm using multimass ion imaging techniques.[5] Two major dissociation channels were observed including (1) $C_6H_3(OH)_2COCH_3 \rightarrow OC_6H_3(OH)COCH_3 + H$ and (2) $C_6H_3(OH)_2COCH_3 \rightarrow C_6H_3(OH)_2 + COCH_3$. The minor channels include $C_6H_3(OH)_2COCH_3 \rightarrow C_6H_3(OH)_2CO + CH_3$ and/or $C_6H_3(OH)_2COCH_3 \rightarrow C_6H_3(OH)_2 + CO + CH_3$. The photofragment translational energy distribution suggests that reaction 1 occurs on an excited state potential that is repulsive along the O−H bond distance.

In this work, we report the 355 nm multiphoton dissociation and multiphoton ionization of DHAP in a molecular beam as well as the 355 nm multiphoton ionization of DHAP in the solid-phase.

II. Experiment

Multiphoton Dissociation. The experimental techniques we employ have been described in detail in our previous work, and only a brief description is given here.[5−8] DHAP molecular beam was formed by flowing ultrapure He carrier gas at pressures of 250 Torr (or Ar at pressure of 300 Torr) through a pulsed nozzle filled with a mixture of solid sample and graphite powder at 90 °C. Molecules in the molecular beam were irradiated by a 355 nm laser beam (Spectra-Physics Lab 190−30, 5 ns pulse duration) and dissociated into neutral fragments. Because of the recoil and center-of-mass velocities, the fragments are distributed on an expanding sphere in flight to the ionization region, where they are ionized by a VUV (118 nm) laser pulse. The dissociation and ionization processes are represented as follows

$$A + nh\nu(355\ \text{nm}) \rightarrow A^*$$

$$A^* \rightarrow B + C$$

$$B + h\nu\,(118\ \text{nm}) \rightarrow B^+ + e^-$$

The distance and time delay between the VUV laser pulse and photolysis laser pulse were set such that the VUV laser beam passed through the center-of-mass of the dissociation products, generating a line segment of photofragment ions. The length of the segment was proportional to the fragment recoil velocity in the center-of-mass frame multiplied by the delay time between the photolysis and ionization laser pulses. To

† Part of the "Vincenzo Aquilanti Festschrift".

* To whom correspondence should be addressed. E-mail address: ckni@po.iams.sinica.edu.tw.

‡ Also at Molecular Science Technology, Taiwan International Graduate Program, Academia Sinica, Taipei, Taiwan.

§ Present address: Institute for Molecular Science, Okazaki, Aichi 444-8585, Japan.

‖ Also at Department of Chemistry, National Taiwan University, Taipei, Taiwan.

⊥ Also at Department of Chemistry, National Tsing Hua University, Hsinchu, Taiwan.

10.1021/jp905111p
Published on Web 09/28/2009

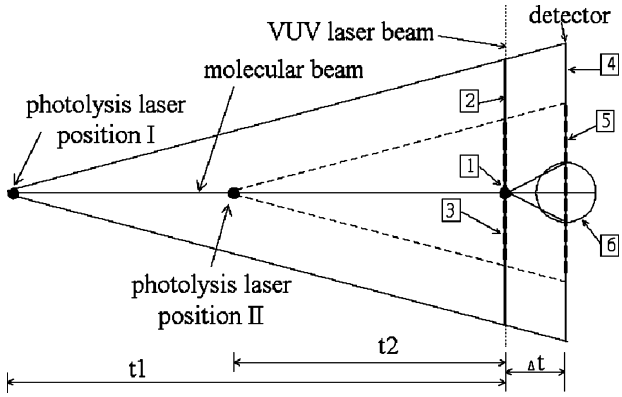

Figure 1. Relationship between the lengths of the line-shape image that resulted from different photolysis laser positions as well as the disklike image from the dissociation after ionization. (1) Represents the crossing point of the molecular beam and the VUV laser beam, where the dissociative ionization occurs. (2,3) Represent the lengths of fragment ion segments created by the VUV laser photoionization from two different photolysis laser positions. (4,5) Represent the lengths of the fragment ion image on the detector from two different photolysis laser positions. (6) Represents the disklike image from dissociative ionization. t_1 and t_2 represent the two different delay times between the photolysis laser pulse and the VUV laser pulse. Δt is the flight time in the mass spectrometer.

separate the different masses within the ion segment, a pulsed electric field was used to extract the ions into a mass spectrometer after ionization. While the mass analysis was being executed in the mass spectrometer, the length of each fragment ion segment continued to expand in the original direction according to its recoil velocity. At the exit port of the mass spectrometer, a two-dimensional ion detector was used to detect the ion positions and intensity distribution. In this two-dimensional detector, one direction was the recoil velocity axis and the other was the mass axis. The image of ion intensity distribution for each mass-to-charge ratio generated from the reactions described above is a line-shape image.

According to the velocity of the molecular beam, it is necessary to change the distance between the photolysis and the VUV laser beams to match the delay time between these two laser pulses thus ensuring that the ionization laser passes through the center-of-mass of the products. Changing of the distance between these two laser beams changes the length of the fragment ion segment in the image. The length of the image increases with increasing delay time (or with increasing distance between UV and VUV laser beams). The relationship between the length of the ion image and the position of the photolysis laser is illustrated in Figure 1.

Molecules that do not dissociated into fragments upon absorption of UV photons retain large internal energy. They remain within the molecular beam and move with the molecular beam velocity to the ionization region where they are ionized by the VUV laser. The wavelength of the VUV laser in this experiment was set at 118.2 nm such that the photon energy was only sufficiently large to ionize parent molecules. The dissociation of parent molecule cations should not occur at the energies left after photoionization. However, dissociation does occur following the VUV laser photoionization for those excited molecules, which absorbed UV photon without dissociation. The reactions can be represented as follows

$$A + nh\nu\,(355\text{ nm}) \rightarrow A^*$$

$$A^* + h\nu\,(118\text{ nm}) \rightarrow B^+ + C + e^-$$

The image of the ion intensity distribution from dissociative ionization differs from the image due to the dissociation products of neutral parent molecules. Because ionization and dissociation occurred at the same position, the image of dissociative ionization was a 2D projection of the photofragment ion's 3D-recoil velocity distribution. It was quite similar in appearance to the image from the conventional ion imaging techniques. It was a disklike image, rather than a line-shape image. The size of image from the dissociative ionization did not change with the delay time between the pump and probe laser pulses.

Ionization of fragments having low ionization potentials resulted in dissociative ionization, generating smaller ionic fragments.

$$A + nh\nu\,(355\text{ nm}) \rightarrow A^*$$

$$A^* \rightarrow B + C$$

$$B + h\nu\,(118\text{ nm}) \rightarrow D^+ + F + e^-$$

The ion image from these reactions was disklike, but the width changed with the delay time. From the shape of the image and its change in width with delay time, images from dissociation of neutral molecules and the respective dissociative ionization of the excited parent molecules and neutral fragments can be distinguished.

Multiphoton Ionization. For our experiment concerning multiphoton ionization, the molecular beam and the 355 nm laser beam were operated under the same conditions as described above. Ions generated by 355 nm laser beam were detected by a linear time-of-flight mass spectrometer.

In the determination of the 355 nm photon number dependence, the change in laser beam fluence was achieved by a combination of a half-wave plate and a polarizer. The linear polarized 355 nm laser beam (from the third harmonics of a Nd:YAG laser) was sent to a half-wave plate, and then passed through a polarizer. By rotation of the half-wave plate, we could change the laser fluence and retain the same laser beam intensity profile.

Multiphoton Ionization in Solid Phase. For solid sample preparation, 2,5-dihydroxyacetophenone (2,5-DHAP) was dissolved in acetonitrile (LC/MS grade, Baker) and deionized water to form a 0.05 M sample solution. Approximately 1.2 μL of the sample solution was deposited on the target plate of a MALDI TOF mass spectrometer (MTP384 target plate polished steel, Ultraflex II, Bruker Daltonik GmbH, Bremen, Germany) and dried under vacuum for analysis. Mass analysis was carried out in both positive and negative ion modes with an acceleration voltage of 25 kV using pulsed ion extraction in reflection mode and with external mass calibration. Each spectrum obtained was the sum of 1000 laser shots.

Calculation Method. We used ab initio methods to calculate geometries and energies of various isomers, transition states, and dissociation products in the ground electronic state. In the calculation, the geometries were optimized at the hybrid density functional B3LYP/6-31G* level and the energies were calculated using G3 model chemistry scheme.

Results and Discussion

A. Multiphoton Ionization in a Molecular Beam. ***Total Ions.*** The time-of-fight (TOF) mass spectrum of the ions generated from 355 nm multiphoton ionization of DHAP in a

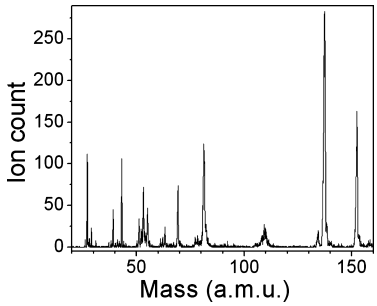

Figure 2. Time-of-flight mass spectrum from 355 nm multiphoton ionization of DHAP.

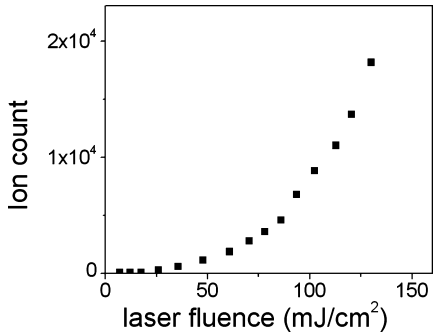

Figure 3. Total ion count generated from 355 nm multiphoton ionization as a function of 355 nm laser fluence.

TABLE I: Photon Number Dependences of Multiphoton Ionization and Dissociation

Multiphoton Ionization									
m/e	152	137	134	109	81	78	77	69	63
slope	2.2	3.7	2.7	4.1	3.8	3.6	3.9	4.0	4.8
m/e	55	53	51	43	39	27			
slope	4.2	4.8	5.8	4.2	4.6	5.3			
Multiphoton Dissociation									
m/e	137	134	109	81	53	52	43	27	15
slope	0.8	0.7	1.4	1.6	1.7	2	1.4	1.4	1.5

Slopes were obtained for the 355 nm laser fluence in the region 3.3−150 mJ/cm^2.

molecular beam is shown in Figure 2. Ions of m/e = 152, 137, 81, 69, 53, 43, and 27 show relatively large intensities whereas ions of m/e = 134, 110, 109, 108, 78, 77, 63, 55, 52, 51, 39 exhibit relatively small intensities. The ion intensity as a function of laser fluence in the region 3.4−130 mJ/cm^2 was studied to investigate the photon number dependence of these ionization processes. Figure 3 shows that the total number of ions increases rapidly with increasing laser fluence.

Parent Ions. Photon number dependences of ion intensities are shown in Table I. The slopes obtained from the plot of ln(ion intensity) as a function of ln(laser fluence) provide the information concerning absorption of photon number. However, the current study investigates the multiphoton absorption processes under large laser fluence; saturation of the absorption could happen in any transition. As a consequence, the actual photon number absorbed to generate these ions can be easily underestimated from the measurements. The slopes are generally not integer-valued due to partial saturation of the absorption. Integers close to the slope values only indicate the minimum photon number required to produce the corresponding ions.

Ion m/e = 152 is parent ion. The slope at small laser fluence region is 2.2, indicating that 2 or 3 photons are required to generate this ion. Vertical and adiabatic ionization potentials of DHAP from our ab initio calculation are 8.3 and 8.1 eV, respectively. The adiabatic ionization potential is close to that for various chromophores, phenol (8.5 eV),[9] *m*-, *o*-, *p*-dihydroxybenzene (8.2, 8.1, and 7.9 eV),[10,11] acetophenone (9.3 eV),[12] *m*-, *p*-acetylphenol (8.7 eV).[13,14] The ionization potential suggests that absorption of three photons is needed to generate ion m/e = 152. The slope value indicates that part of the three-photon absorption process is saturated even in the low laser fluence region. Further saturation was observed in the high laser fluence region.

Ionic Fragments. Ion m/e = 137 corresponds to the dissociative ionization $C_6H_3(OH)_2COCH_3 + nh\nu$ (355 nm) → $C_6H_3(OH)_2CO^+$ (m/e = 137) + CH_3. The heat of reaction from our calculation is ΔH = 10.1−11 eV, depending on the conformers of $C_6H_3(OH)_2CO^+$. This indicates that the generation of ion m/e = 137 requires 3−4 photons. Ions m/e=137 have the largest intensity and this reaction is the major multiphoton ionization channel of DHAP in the molecular beam.

Ion m/e = 134 represents the dissociative ionization reactions (1) $C_6H_3(OH)_2COCH_3 + nh\nu$ (355 nm) → $C_6H_3(OH)OCCH_2^+$ (m/e = 134) + H_2O or (2) $C_6H_2(OH)COCH_3^+$ (m/e = 134) + H_2O. The heats of reaction are ΔH = 10.5 and 12.2 eV respectively. The first reaction includes the ionization, and then H atom transfer from the CH_3 group to the oxygen of the CO group prior to dissociation. The H atom migration has a barrier height of approximately 3 eV relative to the parent cation (adiabatic ionization energy 8.1 eV). Ion intensity of m/e = 134 is small and the reaction is a minor channel among various dissociative ionization processes.

Ion m/e = 109 results from the dissociative ionization $C_6H_3(OH)_2COCH_3 + nh\nu$ → $C_6H_3(OH)_2^+$ (m/e = 109) + $COCH_3$. The heat of reaction is ΔH = 12.8 eV. Another possibility is the dissociation from cation m/e = 137, $C_6H_3(OH)_2CO^+$ (m/e = 137) → $C_6H_3(OH)_2^+$ (m/e = 109) + CO.

In addition to m/e = 109, we also observed small signal at m/e = 108. It is likely the result from the cracking of $C_6H_3(OH)_2^+$ due to the additional H atom loss. The other possibility is CH_4 elimination followed by additional CO loss. However, we did not observe the ions corresponding to CH_4 elimination. These ions all have very large kinetic energy, as shown in the broadening of the peaks in TOF mass spectrum.

Ion m/e = 43 is from the reaction $C_6H_3(OH)_2COCH_3 + nh\nu$ (355 nm) → $C_6H_3(OH)_2$ + $COCH_3^+$ (m/e = 43). The heat of reaction is ΔH = 11.6 eV. The ion can also be produced from the reaction $C_6H_3(OH)_2COCH_3 + nh\nu$ (355 nm) → $C_6H_4O(OH)$ + $COCH_3^+$ (m = 43). The heat of reaction is 10.3 eV with a barrier height of 10.7 eV.

Ion m/e = 81 can be produced from the secondary dissociation of cation m/e = 109 ($C_6H_3(OH)_2^+$ or $C_6H_3O(OH)^+$ from $COCH_3$ elimination) → $C_5H_4(OH)^+$ (m/e = 81) + CO. Ion m/e = 81 can also be produced from the secondary dissociation of neutral fragment $C_6H_3(OH)_2$ or $C_6H_4O(OH)$ (from $COCH_3$ elimination) → $C_5H_4(OH)$ (m = 81) + CO, followed by multiphoton ionization of $C_5H_4(OH)$ (m = 81) by additional 355 nm photons. These secondary reactions have relatively low barrier heights, 2.2 and 2.4 eV for the cation ($C_6H_3O(OH)^+$) and the neutral fragment ($C_6H_4O(OH)$), respectively. Ion m/e = 53 can be generated by additional CO elimination from fragment m = 81. This includes the cation $C_5H_4(OH)^+$ (m/e = 81) → $C_4H_5^+$ (m/e = 53) + CO and the neutral fragment $C_5H_4(OH)$ (m = 81) → C_4H_5 (m = 53) + CO followed by multiphoton ionization. The barrier heights of these additional CO elimination reactions using ab initio calculation were found

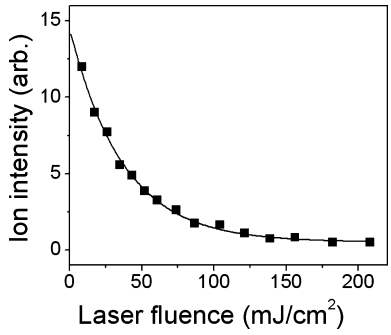

Figure 4. Concentration of unexcited parent molecules left in the molecular beam after the irradiation by various fluence of 355 nm laser beam (solid square). Unexcited parent molecules were detected by VUV (118 nm) photoionization 100 ns after the irradiation by the 355 nm laser beam. The solid line represents the fit to eq 1.

to be 2.9 and 2.4 eV, respectively. Ion $m/e = 52$ and 51 may result from the additional H atom loss from ion $m/e = 53$.

The remaining ions include $m/e = 110$, 78, 77, 69, 55, 51, 39, and 27. Generation of these ions includes many isomerization and dissociation processes. Some of these involve complicated aromatic ring-openings. For example, a possible reaction to generate ion $m/e = 69$ includes the migration of CH_3 to the aromatic ring and the elimination of CO, $C_6H_3(OH)_2COCH_3^+ \rightarrow C_6H_3(OH)_2CH_3 + CO$, followed by a ring-opening dissociation, $C_6H_3(OH)_2CH_3^+ \rightarrow C_3H_2OH + C_3H(OH)CH_3^+$ ($m/e = 69$). However, the identification of these isomerization and dissociation processes is not straightforward due to complex reaction pathways. At this moment, we do not have sufficient evidence to propose how these ions are generated.

B. Multiphoton Dissociation in a Molecular Beam. The VUV laser wavelength used in this experiment is 118 nm. The photon energy is large enough to ionize unexcited parent molecules. However, the energy left in the parent ion after ionization is not enough for further dissociation. On the other hand, molecules that absorbed 355 nm photons without dissociating into fragments can easily crack into smaller ionic fragments by VUV photoionization due to large internal energy. Because excited DHAP either dissociates into fragments before photoionization or cracks into smaller ionic fragments by 118 nm photoionization, the parent ion $C_6H_3(OH)_2COCH_3^+$ ($m/e = 152$) generated from 118 nm photoionization under irradiation by the 355 nm laser beam represents parent molecules without absorption of 355 nm photons. Figure 4 shows the parent ion ($m/e = 152$) intensities obtained by 118 nm photoionization as a function of 355 nm laser fluence. Ion intensity decreases to less than 5% when the laser fluence exceeds 130 mJ/cm^2, indicating that only a small fraction of DHAP molecules is left without absorption of 355 nm photons in the region of high laser fluence.

Since DHAP has a large absorption cross section at 355 nm, almost all of the excitation processes start from the resonance excitation of 355 nm. Excitation from nonresonance two-photon (or more than two-photon) absorption must be very small and it can therefore be neglected. As a result, the decrease of unexcited DHAP must start from one-photon absorption and it can be expressed by eq 1

$$-dN = \sigma IN \qquad (1)$$

where N is the concentration of unexcited DHAP, σ is the one-photon 355 nm absorption cross section, and I is the laser fluence. The σ value obtained from the fit of the experimental data in Figure 4 to eq 1 was found to be $\sigma = 1.3(\pm 0.2) \times 10^{-17}$cm^2.

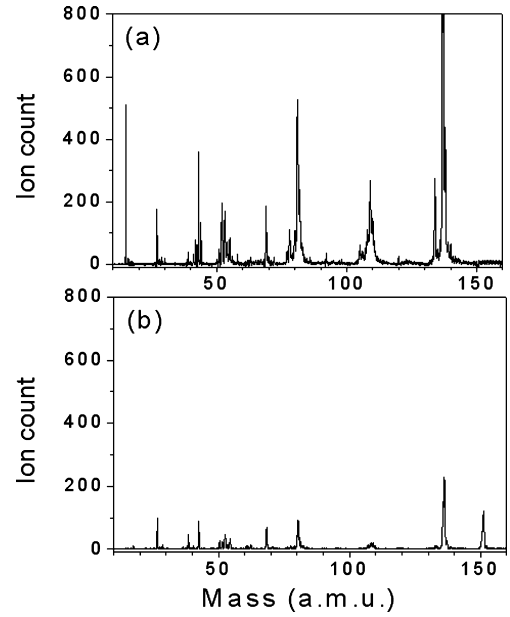

Figure 5. Time-of flight mass spectrum of (a) ions generated by 118 nm photoionization after irradiation of the molecular beam by the 355 nm laser beam. They represent the excited parent molecules as well as the neutral fragments generated by 355 nm photons. The background from 355 nm photoionization as well as the background from 118 nm photoionization have been subtracted. The pump (355 nm) and probe (118 nm) delay time is 100 ns. (b) Ions generated by 355 nm multiphoton ionization.

Total Neutral Fragments. Neutral fragments generated from DHAP after the excitation by 355 nm laser beam were detected by VUV (118 nm) photoionization. Figure 5 shows the ion TOF mass spectrum generated by 118 nm photoionization 100 ns after the irradiation by the 355 nm pump laser pulse at laser fluence 130 mJ/cm^2. This represents the neutral fragments and excited parent molecules generated by 355 nm photons. Ions $m/e = 138$, 137, 134, 110, 109, 82, 81, 69, 53, 52, 43, 27, and 15 have relatively large intensities, whereas ions $m/e = 108$, 80, 78, 77, 55, 54, 51, 42, and 39 have relatively small intensities. Ions $m/e = 138$, 110, and 82 are the ^{13}C isotope of $m/e = 137$, 109, and 81, respectively. Ions generated from 355 nm multiphoton ionization are also shown in the same scale for comparison. It illustrates that ions from 118 nm photoionization of neutral fragments have a total intensity 10 times larger than the ion intensity generated by 355 nm multiphoton ionization. The ions generated by 118 nm photoionization can be expressed by Ion (118 nm) $= P \times \sigma \times l \times C$, where P is the 118 nm photon number per pulse ($P = 10^{11}$ photon/pulse), σ is the 118 nm photoionization cross section, l is the effective width of the molecular beam, and C is the concentration of neutral fragments. The ratio between the number of ions generated from 355 nm ionization, N_1, and the number of neutral fragments produced by 355 nm dissociation, N_2, can be calculated from $R = N_1/N_2 = N_1/(A \times l \times C) = N_1 \times P \times \sigma/(A \times \text{Ion (118 nm)}) = 10^{-6}$. The quantities used to calculate R include the effective overlap area of the 355 nm laser beam and the molecular beam A (= 0.12 cm^2), N_1/Ion (118 nm) = 0.1 from experimental measurement and the estimated average ionization cross section $\sigma = 10^{-17}$cm^2. We find that the number of neutral fragments generated from 355 nm multiphoton absorption is 10^6 times larger than that for ionic fragments. In

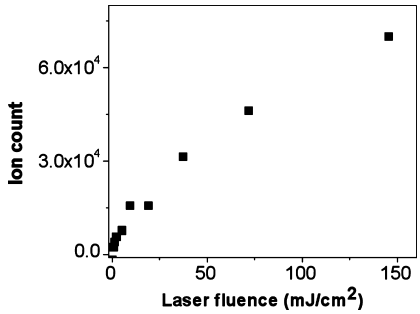

Figure 6. Total number of ions generated by 118 nm photoionization, representing the number of neutral fragments, as a function of 355 nm laser fluence.

other words, the total branching ratio for the various multiphoton ionization channels is only about one part per million at laser fluence 130 mJ/cm^2. Most of the multiphoton excitation results in the dissociation into neutral fragments.

Figure 6 depicts total ions generated by 118 nm photoionization as a function of 355 nm laser fluence. It represents the concentration of neutral fragments generated at various laser fluences. It shows that the total number of neutral fragments increases with increasing the 355 nm laser fluence, but it levels off in the large laser fluence region. By contrast, the total number of ions generated by 355 nm multiphoton ionization increases rapidly as the 355 nm laser fluence increases. This can be rationalized by the fact that most of the parent molecules absorb 355 nm photons in the high laser fluence region. Consequently, few unexcited parent molecules remain to be excited with further increases in the 355 nm laser fluence. Saturation of the absorption results in a leveling off of the total number of neutral fragments.

Dissociative Ionization of Undissociated Excited DHAP. Ion m/e=137 represents $C_6H_3(OH)_2CO^+$. There are two possible mechanisms to generate this ion. One is from 355 nm dissociation, followed by 118 nm ionizations.

$$C_6H_3(OH)_2COCH_3 + nh\nu\,(355\text{ nm}) \rightarrow C_6H_3(OH)_2CO + CH_3 \quad (2a)$$

$$C_6H_3(OH)_2CO + h\nu\,(118\text{ nm}) \rightarrow C_6H_3(OH)_2CO^+\,(m = 137) \quad (2b)$$

One-photon absorption at 355 nm is just enough to overcome the dissociation threshold of reaction 2a (73.6 kcal/mol or 3.1 eV). Absorption of two 355 nm photons will generate fragments with some recoil velocity and internal energy. Fragments with large internal energy may undergo secondary dissociation $C_6H_3(OH)_2CO \rightarrow C_6H_3(OH)_2 + CO$ due to a small dissociation threshold (ΔH = 41.3 kcal/mol) for the process.

The other mechanism includes the absorption of one 355 nm photon. The dissociation rate for excited parent molecules is very small because the energy from one 355 nm photon is just slightly above the dissociation threshold. These molecules would not dissociate into fragments within our observation window. Molecules with large internal energies undergo dissociative ionization by 118 nm photoionization.

$$C_6H_3(OH)_2COCH_3 + h\nu\,(355\text{ nm}) \rightarrow C_6H_3(OH)_2COCH_3^* \quad (3a)$$

$$C_6H_3(OH)_2COCH_3^* + h\nu\,(118\text{ nm}) \rightarrow C_6H_3(OH)_2CO^+\,(m = 137) + CH_3 \quad (3b)$$

Here $C_6H_3(OH)_2COCH_3$* represents the excited parent molecule, absorbing one 355 nm photon without dissociating into fragments before the arrival of the 118 nm laser pulse. The ionization energy of $C_6H_3(OH)_2CO$ is 8.8 eV as determined from our ab initio calculation. The sum of the heats of reactions 3a,b is ΔH = 3.1 + 8.8 = 11.9 eV. The sum of one 355 nm photon energy (3.49 eV) and one 118 nm photon energy (10.49 eV) is high enough to undergo reactions 3a,b. Ion images obtained from different delay time between pump and probe laser pulses allow us to distinguish the ions generated from reaction 2 and reaction 3. Figure 7 shows the image of m/e = 137. We found that the widths of the images obtained at delay time, 7 and 22 μs are the same, which suggests that they are from reaction 3 rather than reaction 2.

The ion count for m/e = 137 as a function of 355 nm laser fluence is shown in Figure 8. It increases in the region smaller than 50 mJ/cm^2, levels off in 50−100 mJ/cm^2, and then decreases beyond 100 mJ/cm^2. The slope given in Figure 8 within the low laser fluence region confirms that ions m/e = 137 results from one-photon absorption, as shown in reaction 3. The decrease of m/e = 137 in the high laser fluence region indicates an increase in two-photon and high photon absorption processes. A comparison of Figure 4 and Figure 8 suggests that at the laser fluence exceeding 150 mJ/cm^2 almost all of the

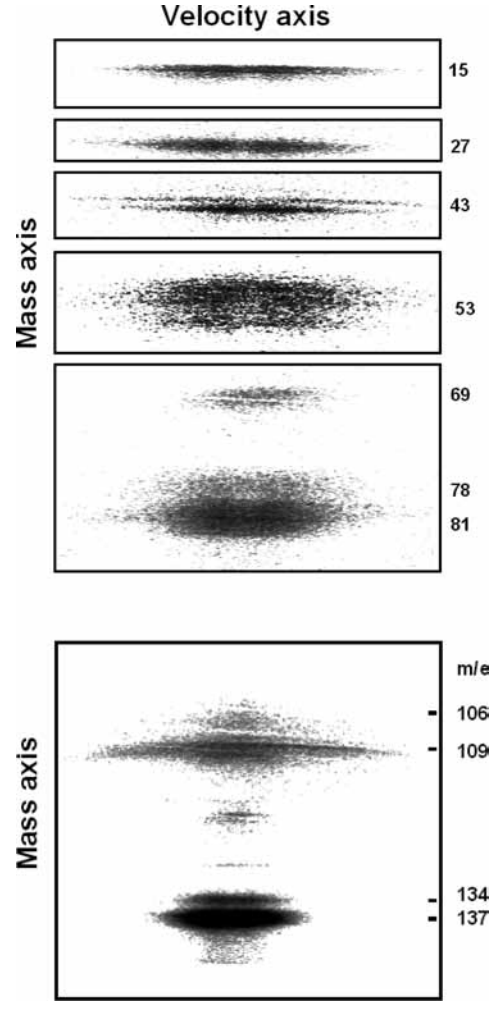

Figure 7. Ion images of various fragments.

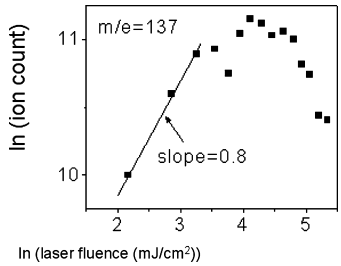

Figure 8. Ion intensity generated from 118 nm photoionization as a function of 355 nm laser fluence.

molecules are excited by 355 nm photons. However, some molecules remain as one 355 nm photon absorber even at 240 mJ/cm^2, as shown by the large value of $m/e = 137$ in the high laser fluence region.

The lifetime of one-photon excited DHAP can be measured from the decay of $m/e = 137$ as a function of pump and probe delay time. It was found that the intensity of $m/e = 137$ does not change within 0−23 μs. We estimate a lifetime for excited DHAP molecules that exceeds 320 μs. This long lifetime indicates that the one-photon excited DHAP molecules either undergo an intersystem crossing to a triplet state or undergo internal conversion to the ground state. Molecules in the triplet state or in the ground state have very small dissociation rates and do not dissociate into fragments within our observation window. Similar slow dissociation rates have been found in benzene and toluene excited by 248 nm photons.[6]

It is also possible that the one-photon excited DHAP molecules represent the excited DHAP after emission of fluorescence. If the vibrational energy retained in DHAP after fluorescence emission is larger than 1.4 eV, these DHAP molecules have enough energy to undergo reaction 3b after being ionized by a 118 nm photon. However, the ion intensity for $m/e = 137$ is only a little smaller than the decrease in the parent ion intensity $m/e = 152$ under 355 nm irradiation. Additionally, the disklike image for $m/e = 137$ is much wider than the molecular beam width. This suggests that if one-photon excited DHAP represents excited DHAP after emission of fluorescence, then the fluorescence quantum yield must be close to one and the vibrational energy left in the ground state after emission of fluorescence needs to be much more than 1.4 eV. At this moment, we do not have further evidence and therefore, this possibility cannot be entirely excluded.

The intensity of ion $m/e = 134$ generated by 118 nm photoionization is 10−15 times smaller than that of $m/e = 137$. However, they share similar properties. The width of the image $m/e = 134$ does not change with delay time. The slope given in Table I suggests that $m/e = 134$ results from one-photon absorption followed by dissociative ionization

$$C_6H_3(OH)_2COCH_3 + h\nu\,(355\text{ nm}) \rightarrow C_6H_3(OH)_2COCH_3^* \quad (4a)$$

$$C_6H_3(OH)_2COCH_3^* + h\nu\,(118\text{ nm}) \rightarrow C_6H_2(OH)COCH_3^+\,(m/e = 134) + H_2O \quad (4b)$$

$C_6H_3(OH)_2COCH_3 \rightarrow C_6H_3(OH)_2CO + CH_3$ and $C_6H_3(OH)_2 + COCH_3$. Ion $m/e = 109$ generated by 118 nm photoionization represents $C_6H_3(OH)_2^+$ or $C_6H_4O(OH)^+$. The image of $m/e = 109$ contains two components. A line-shape image superimposed on a disklike image. However, the widths of both images increase with increasing the delay time. The disklike image represents the dissociative ionization of the heavy fragment $C_6H_3(OH)_2CO$

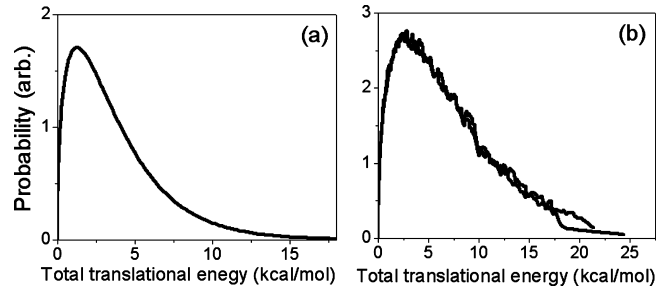

Figure 9. Photofragment translational energy distribution of reaction (a) $C_6H_3(OH)_2COCH_3 + 2h\nu$ (355 nm) → $C_6H_3(OH)_2CO + CH_3$. (b) $C_6H_3(OH)_2COCH_3 + 2h\nu$ (355 nm) → $C_6H_3(OH)_2 + COCH_3$.

$$C_6H_3(OH)_2COCH_3 + nh\nu\,(355\text{ nm}) \rightarrow C_6H_3(OH)_2CO + CH_3 \quad (5a)$$

$$C_6H_3(OH)_2CO + h\nu\,(118\text{nm}) \rightarrow C_6H_3(OH)_2^+\,(m/e = 109) + CO \quad (5b)$$

A match of momentum distributions between $m/e = 15$ (CH_3) and the disklike component of $m/e = 109$ (using $m = 137$ in the momentum calculation) confirms that they are from dissociation channel 5a. The photofragment translational energy distribution of reaction 5a, as illustrated in Figure 9a, shows that the maximum translational energy is smaller than the available energy from two 355 nm photons.

The line shape image of $m/e = 109$ corresponds to dissociation from neutral parent molecules.

$$C_6H_3(OH)_2COCH_3 + nh\nu\,(355\text{ nm}) \rightarrow C_6H_3(OH)_2 + COCH_3 \quad (6a)$$

$$C_6H_3(OH)_2 + h\nu\,(118\text{ nm}) \rightarrow C_6H_3(OH)_2^+\,(m/e = 109) \quad (6b)$$

The dissociation threshold of reaction 6a is $\Delta H = 106.8$ kcal/mol (4.6 eV). It requires at least two photons of 355 nm for reaction 6a to occur.

The image of ions $m/e = 81$ also contains two components as illustrated in Figure 8. However, the line-shape image is much weaker than the disklike image. The line-shape image represents a secondary dissociation following reaction 6a

$$C_6H_3(OH)_2 \rightarrow C_5H_4(OH) + CO \quad (\Delta H = 55\text{ kcal/mol}) \quad (6c)$$

The component of disklike image results from the cracking of the heavy fragment $C_6H_3(OH)_2$.

$$C_6H_3(OH)_2\,(m = 109) + h\nu\,(118\text{ nm}) \rightarrow C_5H_4(OH)^+\,(m/e = 81) + CO \quad (6d)$$

Ion $m/e = 43$ represents $COCH_3^+$, resulting from reaction 6a followed by VUV ionization. The momentum distribution

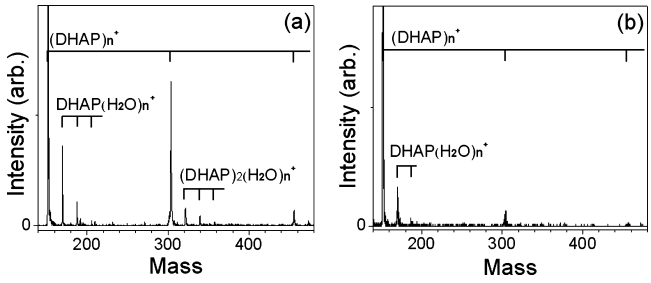

Figure 10. Mass spectrum of clusters in the molecular beam obtained from (a) 118 nm photoionization (b) 355 nm multiphoton ionization.

of $m/e = 43$ matches with the momentum distribution from the sum of the line shape image of $m/e = 109$ and the disklike image of $m/e = 81$ (using $m = 109$ in the momentum calculation). It confirms reaction 6a,b,d. The photofragment translational energy distribution, as shown in Figure 9b, denotes that the release of the available energy into translational energy is small.

The production of ions with $m/e = 109$ from one 355 nm photon absorption followed by dissociative ionization by 118 nm photoionization is energetically allowed

$$C_6H_3(OH)_2COCH_3 + h\nu\,(355\text{ nm}) \rightarrow C_6H_3(OH)_2COCH_3^* \quad (7a)$$

$$C_6H_3(OH)_2COCH_3^* + h\nu\,(118\text{ nm}) \rightarrow C_6H_3(OH)_2^+\,(m/e = 109) + COCH_3 \quad (7b)$$

$$C_6H_3(OH)_2COCH_3^* + h\nu\,(118\text{ nm}) \rightarrow C_6H_3(OH)_2^+\,(m/e = 109) + CO + CH_3 \quad (7c)$$

However, we did not observe a disklike image of $m/e = 109$, which is a width that does not change with delay time. It suggests that either the intensity from reaction 7 is very small and it is buried in the large intensity from reaction 6, or that reaction 7 does not occur.

Ion $m/e = 53$ has a disklike image and the width increases with the delay time. It is from the cracking of $m/e = 81$ upon photoionization.

$$C_5H_4(OH)\,(m/e = 81) + h\nu\,(118\text{ nm}) \rightarrow C_4H_5^+(m/e = 53) + CO$$

The remaining ions include $m/e = 27$, 44, 51, 52, and 69. They represent the fragments from complicated aromatic ring-opening dissociations, although the intensities are small. Currently, we cannot establish how these fragments are produced.

C. Photoionization of DHAP Clusters in a Molecular Beam and DHAP in Solid Phase. In changing the carrier gas from He (250 Torr) to Ar (300 Torr), various clusters formed, that is, dimers, trimers, complexes of DHAP and water $(DHAP)(H_2O)_n$, and complexes of DHAP and Ar $(DHAP)Ar_n$, were formed. These complexes can be observed from the mass spectrum obtained by 118 nm photoionization, as shown in Figure 10. The formation of water complex is likely due to the small amount of water in the sample gas line. However, the mass spectrum obtained from 355 nm multiphoton ionization under the same molecular beam conditions gives different results. The ratio of clusters to monomer decreases as the laser beam changes from 118 to 355 nm. Most of these clusters tend to dissociate into monomer when they are ionized by 355 nm laser beam.

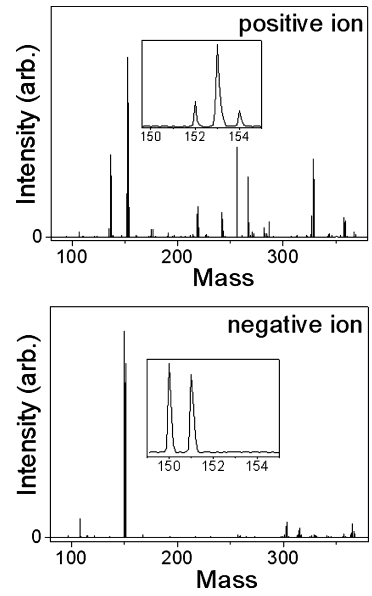

Figure 11. 355 nm matrix-assisted laser desorption/ionization mass spectrum of solid-phase DHAP.

Protonated monomer and negatively charged ions of the matrix compounds are frequently observed in MALDI experiments.[1] Almost equal amount of protonated DHAP and negatively charged ion from the loss a proton were observed in MALDI experiments using 355 nm laser beam, as shown in Figure 11. We also searched for protonated DHAP and negatively charged ions from the 355 nm multiphoton ionization of clusters in the molecular beam. We did not find the corresponding ions. This suggests that protonated DHAP and negatively charged DHAP generated in MALDI experiments does not simply result, for example, from the proton transfer reactions of the clusters in the gas phase such as the reaction described below.

$$(DHAP)_2 + nh\nu\,(355\text{ nm}) \rightarrow (DHAP)H^+ + (DHAP - 1)^-$$

Complicated reactions must occur to generate these ions in MALDI experiments.

In summary, when DHAP is exposed to 355 nm irradiation, dissociation into neutral fragment, ionization, and dissociative ionization following photoexcitation occurs. Nearly all DHAP molecules absorb at least one photon under irradiation of the 355 nm laser beam when the fluence is larger than 130 mJ/cm^2. Molecules absorbing two photons dissociate into fragments through major channels, $C_6H_3(OH)_2COCH_3 \rightarrow C_6H_3(OH)_2CO + CH_3$ and $C_6H_3(OH)_2COCH_3 \rightarrow C_6H_3(OH)_2 + COCH_3$. Molecules absorbing three photons become parent ions. Those molecules, which absorb more than three photons, result in ionic fragments. In the laser intensity region we employed in this work, most DHAP molecules dissociated into neutral fragments. The concentration ratio of ions (parent ions and ionic fragments) to neutral fragments is about 10^{-6}:1. We observed almost equal amount of protonated DHAP and negatively charged DHAP with a single H atom lost in solid-phase experiment. However, neither protonated DHAP nor negatively charged ions were observed from the photoionization of DHAP clusters in the molecular beam. Our findings indicate that the photoionization

occurring in the gas phase after DHAP vaporizes from the solid phase may not play an important role in the MALDI process.

References and Notes

(1) Krause, J.; Stoeckli, M.; Schlunegger, U. P. *Rapid Commun. Mass Spectrom.* **1996**, *10*, 1927.

(2) Ehring, H.; Karas, M.; Hillenkamp, F. *Org. Mass Spectrom.* **1992**, *27*, 427.

(3) Karas, M.; Kruger, R. *Chem. Rev.* **2003**, *103*, 427.

(4) Chang, W. C.; Huang, L. C. L.; Wang, Y. S.; Peng, W. P.; Chang, H. C.; Hsu, N. Y.; Yang, W. B.; Chen, C. H. *Anal. Chim. Acta* **2007**, *582*, 1.

(5) Morisawa, Y.; Dyakov, Y. A.; Tseng, C. M.; Lee, Y. T.; Ni, C. K. *J. Phys. Chem. A* **2009**, *113*, 97.

(6) Tsai, S. T.; Lin, C. K.; Lee, Y. T.; Ni, C. K. *J. Chem. Phys.* **2000**, *113*, 67.

(7) Tsai, S. T.; Lin, C. K.; Lee, Y. T.; Ni, C. K. *Rev. Sci. Instrum.* **2001**, *72*, 1963.

(8) Ni, C. K.; Lee, Y. T. *Int. Rev. Phys. Chem.* **2004**, *23*, 187.

(9) Lipert, R. J.; Colson, S. D. *J. Chem. Phys.* **1990**, *92*, 3240.

(10) Oikawa, A.; Abe, H.; Mikami, N.; Ito, M. *Chem. Phys. Lett.* **1985**, *116*, 50.

(11) Palmer, M. H.; Moyes, W.; Speirs, M.; Ridyard, J. N. A. *J. Mol. Struct.* **1979**, *52*, 293.

(12) McLoughlin, R. G.; Traeger, J. C. *Org. Mass Spectrom.* **1979**, *14*, 434.

(13) Pignataro, S.; Foffani, A.; Innorta, G.; Distefano, G. *Z. Phys. Chem. (Frankfurt)* **1966**, *49*, 291.

(14) Foffani, A.; Pignataro, S.; Cantone, B.; Grasso, F. *Z. Phys. Chem. (Frankfurt)* **1964**, *42*, 221.

JP905111P